Input-Specific NMDAR-Dependent Potentiation of Dendritic GABAergic Inhibition

Highlights

- Activation of NMDARs potentiates GABAergic inhibition from SOM-INs

- Dendritic, but not perisomatic, GABAergic synapses are sensitive to CaMKIIα activity

- GABAergic potentiation requires expression of the $GABA_AR$ β2 subunit

- Loss of NMDARs alters the balance of inhibition along the somatodendritic axis

Authors

Chiayu Q. Chiu, James S. Martenson, Maya Yamazaki, ..., Susumu Tomita, Steven J. Tavalin, Michael J. Higley

Correspondence

m.higley@yale.edu

In Brief

Using electrophysiology and optogenetics, Chiu et al. show that activation of NMDA-type glutamate receptors selectively potentiates inhibition from somatostatin-expressing interneurons onto cortical pyramidal cells. This work suggests a mechanism for regulating the balance of excitation and inhibition in neuronal dendrites.

CellPress

Input-Specific NMDAR-Dependent Potentiation of Dendritic GABAergic Inhibition

Chiayu Q. Chiu,[1,2] James S. Martenson,[1,3] Maya Yamazaki,[4] Rie Natsume,[4] Kenji Sakimura,[4] Susumu Tomita,[1,3] Steven J. Tavalin,[5] and Michael J. Higley[1,6,*]

[1]Department of Neuroscience, Program in Cellular Neuroscience, Neurodegeneration, and Repair, Kavli Institute for Neuroscience, Yale University School of Medicine, New Haven, CT 06510, USA
[2]Centro Interdisciplinario de Neurociencia de Valparaíso, Universidad de Valparaíso, Valparaíso 2360102, Chile
[3]Department of Cellular and Molecular Physiology, Yale University School of Medicine, New Haven, CT 06510, USA
[4]Department of Cellular Neurobiology, Brain Research Institute, Niigata University, Niigata 951-8585, Japan
[5]Department of Pharmacology, University of Tennessee Health Science Center, Memphis, TN 38103, USA
[6]Lead Contact
*Correspondence: m.higley@yale.edu
https://doi.org/10.1016/j.neuron.2017.12.032

SUMMARY

Preservation of a balance between synaptic excitation and inhibition is critical for normal brain function. A number of homeostatic cellular mechanisms have been suggested to play a role in maintaining this balance, including long-term plasticity of GABAergic inhibitory synapses. Many previous studies have demonstrated a coupling of postsynaptic spiking with modification of perisomatic inhibition. Here, we demonstrate that activation of NMDA-type glutamate receptors leads to input-specific long-term potentiation of dendritic inhibition mediated by somatostatin-expressing interneurons. This form of plasticity is expressed postsynaptically and requires both CaMKIIα and the β2 subunit of the GABA-A receptor. Importantly, this process may function to preserve dendritic inhibition, as genetic deletion of NMDAR signaling results in a selective weakening of dendritic inhibition. Overall, our results reveal a new mechanism for linking excitatory and inhibitory input in neuronal dendrites and provide novel insight into the homeostatic regulation of synaptic transmission in cortical circuits.

INTRODUCTION

The balance of synaptic excitation and inhibition is central to normal brain function and is disrupted in a variety of neurodevelopmental disorders (Gogolla et al., 2009; Isaacson and Scanziani, 2011; Lewis and Hashimoto, 2007). In the neocortex, this balance is hypothesized to be maintained via an array of mechanisms that regulate synaptic strength and excitability (Kullmann et al., 2012; Malenka and Bear, 2004; Turrigiano, 2011). Mechanistic studies of synaptic plasticity have largely focused on potentiation and depression of excitatory glutamatergic connections. More recently, plasticity of inhibitory GABAergic synapses has also begun to receive attention, although the underlying cellular targets and molecular mechanisms are less well understood (Castillo et al., 2011; Kullmann et al., 2012).

A major challenge to understanding the contribution of inhibitory plasticity to brain development and function is the diversity of cortical GABAergic interneurons (INs) (Ascoli et al., 2008). Recent work suggests three principal groups: cells co-expressing the calcium (Ca^{2+})-binding protein parvalbumin (PV), the peptide transmitter somatostatin (SOM), or the serotonin 5HT3a receptor (Rudy et al., 2011). The latter class includes the vasoactive intestinal peptide (VIP)-expressing cells. PV-INs make inhibitory contacts onto the perisomatic and proximal dendritic regions of excitatory pyramidal neurons (PNs) and exert well-documented control over the magnitude and timing of PN spike output (Cardin et al., 2009; Pouille and Scanziani, 2001). SOM-INs contact dendritic arbors, where they regulate Ca^{2+} signaling, synaptic integration, and dendritic spikes (Chiu et al., 2013; Murayama et al., 2009). VIP-INs largely, though not exclusively, target other INs and may drive state-dependent disinhibition of PNs (Fu et al., 2014; Pfeffer et al., 2013).

Recent evidence using two-photon imaging of fluorescently tagged inhibitory synapses *in vivo* suggests distinct learning rules for different populations of GABAergic inputs (Chen et al., 2012; Villa et al., 2016). In particular, inhibitory synapses onto dendritic spines, potentially formed by SOM-INs (Chiu et al., 2013), appear to be particularly plastic, as their basal turnover and response to sensory deprivation is significantly more dynamic than those onto dendritic shafts (Chen et al., 2012; van Versendaal et al., 2012). These findings suggest the intriguing possibility of GABAergic circuit-specific plasticity.

Notably, most studies of GABAergic plasticity have implicated perisomatic inhibition as a key locus for regulation. For example, synapses formed by PV-INs in primary visual cortex selectively exhibit long-term potentiation (iLTP) in response to activity-dependent release of nitric oxide by postsynaptic PNs (Lourenço et al., 2014), and inputs from fast-spiking, putative PV-INs onto layer 4 PNs are selectively modified by visual experience (Maffei et al., 2006). Similarly, cholecystokinin (CCK)-expressing basket cells targeting proximal somatodendritic regions in the hippocampus are particularly sensitive to retrograde endocannabinoid

signaling (Lee et al., 2010). Finally, Purkinje cell-targeting basket cells in the cerebellum exhibit iLTP in response to postsynaptic Ca^{2+} signaling (He et al., 2015). It is less clear whether GABAergic inputs to neuronal dendrites are regulated by similar mechanisms. Because excitatory and inhibitory synapses are in close proximity within dendritic compartments, glutamatergic activity may intimately shape dendritic inhibition. Indeed, previous studies in cultured hippocampal neurons, where circuit architecture is not preserved, suggested links between Ca^{2+} influx through NMDA-type glutamate receptors (NMDARs) and GABAergic synaptic function (Marsden et al., 2007; Petrini et al., 2014).

To determine whether glutamatergic signaling can directly influence inhibitory synaptic potency in intact cortical circuits, we utilized optogenetic stimulation of targeted GABAergic IN populations paired with either pharmacological or optogenetic activation of postsynaptic NMDARs. Our results show the remarkable finding that Ca^{2+} influx through NMDARs selectively drives iLTP of SOM-IN synapses, while inputs from PV-INs and VIP-INs are unaffected. Indeed, activation of the type 2α Ca^{2+} and calmodulin-dependent kinase (CaMKIIα) selectively induces potentiation of SOM-IN, but not PV-IN, synapses. This form of plasticity is expressed postsynaptically and requires the β2 subunit of the $GABA_A$ receptor, which we show functions preferentially at SOM-IN synapses. Finally, we show that genetic disruption of NMDAR activity leads to distinct consequences for perisomatic and dendritic inhibition. These results suggest functional heterogeneity of GABAergic synapses in different somatodendritic compartments, which may have direct consequences for activity-dependent, homeostatic balancing of excitatory and inhibitory circuits.

RESULTS

To examine the impact of glutamatergic signaling on specific subsets of GABAergic synapses, we used a viral vector to conditionally express EYFP-fused channelrhodopsin-2 (ChR2) in three populations of GABAergic INs (SOM-, PV-, or VIP-INs) within the mouse medial prefrontal cortex (Figures 1A–1C, left). We selectively activated ChR2-expressing cells in acute slices with brief pulses of 473 nm light while monitoring the corresponding inhibitory postsynaptic currents (IPSCs) in nearby L2/3 PNs (Figures 1A–1C, middle). In these experiments, PNs were loaded with chloride through the patch pipette to obtain detectable inward IPSCs at a holding potential of −70 mV. After obtaining a stable baseline, 20 μM NMDA was bath applied for 2 min and rapidly washed out (Figures 1A–1C, right). In all experiments, inhibitory currents disappeared during NMDA wash-in and reappeared in the first 2 min after NMDA cessation, presumably due to NMDA-induced depolarization block of presynaptic neurons. Experiments using SOM-INs revealed that chemical activation of NMDARs produced a significant potentiation of optically evoked IPSCs (SOM-IPSCs), reaching a plateau ∼20 min after NMDA washout (171% ± 18%, n = 8 cells, p = 0.02; Figures 1A and 1E). This rise was not correlated with changes in series or membrane resistance (Figure 1D). Surprisingly, inhibitory responses mediated by either PV-INs (PV-IPSCs) or VIP-INs (VIP-IPSCs) did not exhibit potentiation following NMDAR activa-

tion, only recovering back to baseline (PV: 105% ± 5%, n = 7 cells, p = 0.78; VIP: 91% ± 8%, n = 8 cells, p = 0.20). Thus, our results demonstrate that glutamatergic signaling can drive iLTP in the neocortex, but this phenomenon is specific to a subpopulation of GABAergic synapses.

Bath application of NMDA may increase neuronal activity in the slice, leading to release of unspecified transmitters that might mediate iLTP. Therefore, we determined the requirement for postsynaptic NMDAR signaling in the recorded PN by loading cells with the NMDAR blocker MK-801 through the patch pipette. This manipulation abolished iLTP of SOM-IPSCs (109% ± 8%, n = 7 cells, p = 0.005 compared to control; Figure 1E). In particular, NMDARs containing GluN2B subunits are required for iLTP, as bath application of the specific antagonist ifenprodil also blocked potentiation (74% ± 11%, n = 5 cells, p = 0.02 compared to control; Figure 1E). Moreover, chelating postsynaptic Ca^{2+} by including BAPTA in the patch pipette also blocked iLTP (83% ± 10%, n = 4 cells, p = 0.001 compared to control; Figure 1E). These results strongly indicate that iLTP is induced cell autonomously by the activation of postsynaptic NMDARs and subsequent Ca^{2+} influx.

Additional pharmacological assays revealed that blockade of either $GABA_B$ receptors (CGP-55845: 177% ± 33%, n = 3 cells, p = 0.84) or L-type voltage-gated Ca^{2+} channels (nimodipine: 171% ± 23%, n = 4 cells, p = 0.60) did not reduce the magnitude of iLTP compared to controls. In addition, we confirmed that iLTP is also observed when monitoring outward currents at +10 mV in cells containing a physiological chloride concentration (low chloride: 165% ± 14%, n = 6 cells, p = 0.89 compared to high chloride control), arguing that plasticity is not due to a change in the $GABA_A$ reversal potential and is not an artifact of chloride loading (Figure 1E). Notably, we cannot rule out a direct contribution of $GABA_A$R-mediated signaling to the induction of iLTP, though the lack of detectable IPSCs during NMDA exposure suggests little, if any, GABA release during the induction period.

NMDAR-dependent plasticity is often linked to Ca^{2+}-dependent activation of CaMKIIα. Therefore, we tested the role of this kinase in iLTP. Both extracellular blockade with the antagonist KN-62 and intracellular blockade by cell loading with autocamtide-2-related inhibitory peptide (AIP) abolished iLTP of SOM-IPSCs (control: 156% ± 16%, n = 8 cells; KN-62: 91% ± 5%, n = 7 cells, p = 0.0003; AIP: 100% ± 5%, n = 8 cells, p = 0.0002; Figures 2A and 2B).

The lack of CaMKIIα-dependent iLTP at PV-IN synapses might reflect either absence of kinase at these perisomatic inputs or insensitivity to its actions. To distinguish between these possibilities, we examined whether direct activation of CaMKIIα is sufficient to potentiate IPSCs. In initial experiments, cells were loaded with Ca^{2+} and calmodulin through the patch pipette in the presence of the calcineurin antagonist cyclosporine A (Wang and Kelly, 1995). We began by recording IPSCs evoked by optical stimulation of SOM-INs immediately after breaking into the cell and observed a steady augmentation of response amplitude (213% ± 16%, n = 10, p = 0.002; Figures 2C and 2D), which was not observed in cells loaded with control pipette solution (122% ± 10%, n = 7, p = 0.22). KN-62 abolished the effect of loading Ca^{2+}/calmodulin (103% ± 11%, n = 6, p = 0.0005; Figure 2D), suggesting that direct activation of
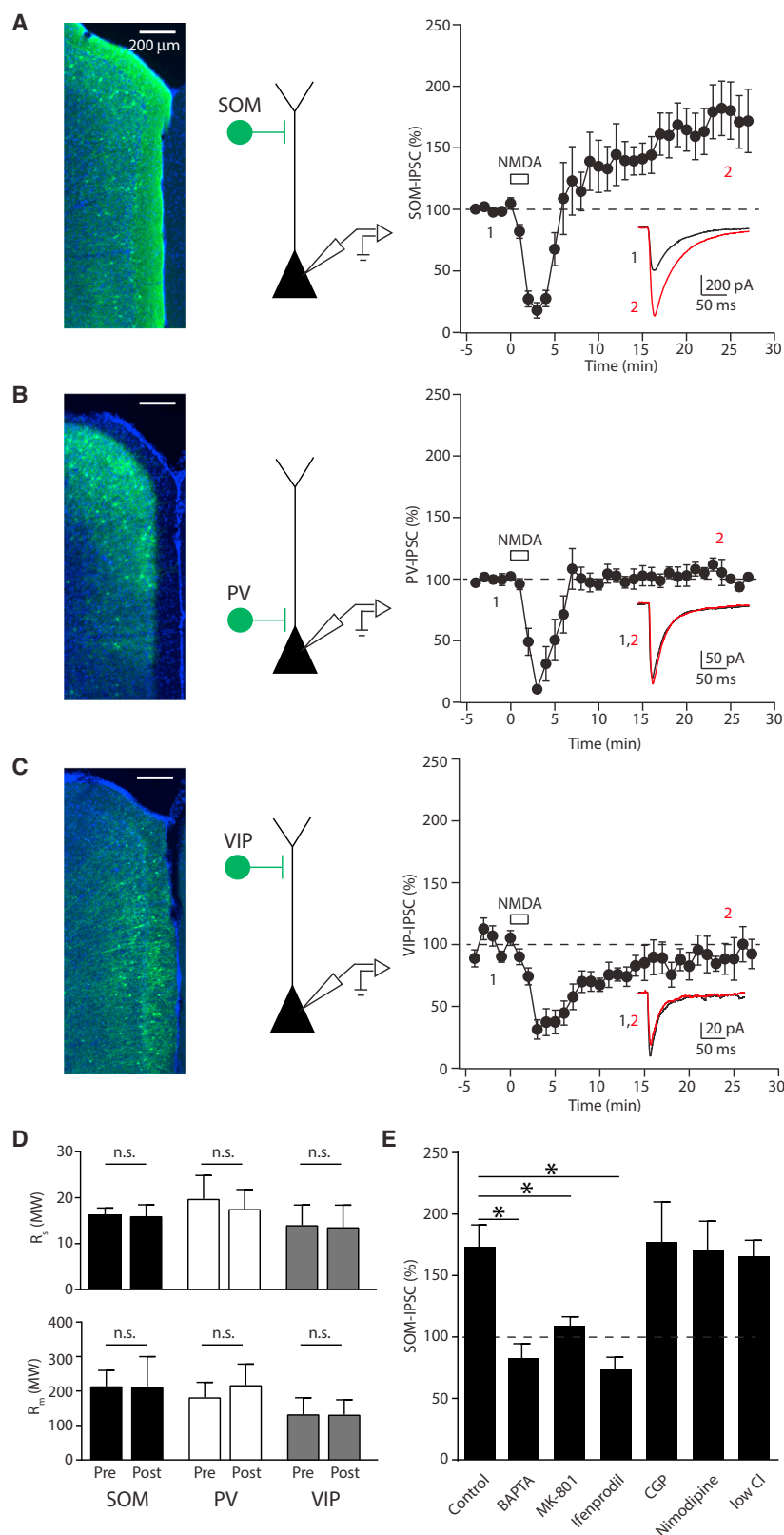
Figure 1. NMDA Selectively Potentiates GABAer-gic Inhibition Mediated by SOM-INs

(A) Left: epifluorescence image of ChR2-EYFP (green) expression and DAPI (blue) in the prefrontal cortex of a SOM-Cre mouse. Middle: schematic of the recording and stimulation configuration. Right: time course of inhibitory postsynaptic currents in L2/3 pyramidal cells evoked by photo-activation of SOM-INs before and after brief application of 20 μM NMDA. Average IPSC traces obtained before (black) and after (red) NMDA exposure from a single experiment at time points indicated are shown in the inset.

(B) Same as in (A) but for photo-activation of PV-INs.

(C) Same as in (A) but for photo-activation of VIP-INs.

(D) Series (top) and membrane (bottom) resistance are unchanged after brief NMDA exposure for all three groups.

(E) Summary plot of the involvement of different Ca^{2+} sources and receptors on iLTP of SOM-IN inputs. Data are represented as mean ± SEM. Asterisks denote p value of <0.05, Mann-Whitney test.
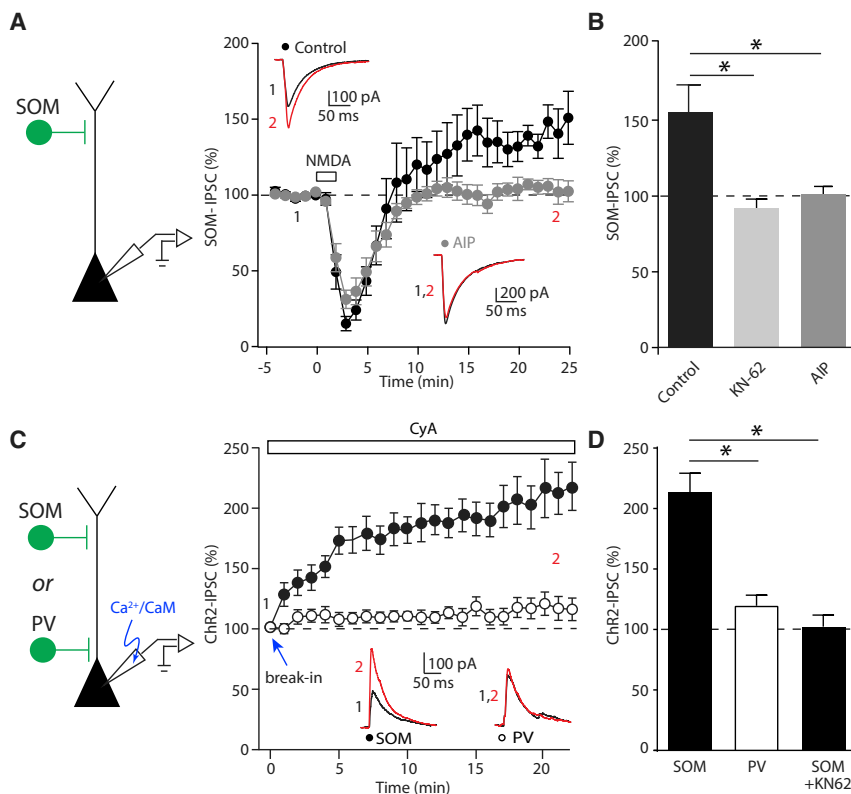
Figure 2. CaMKIIα Activity Mediates iLTP of Dendritic GABAergic Inhibition

(A) Time course of inhibitory postsynaptic currents evoked by photo-activation of SOM-INs before and after NMDA application using control internal solution or patch solution loaded with AIP. Average IPSC traces obtained before (black) and after (red) NMDA exposure from a single experiment at time points indicated are shown in the insets.

(B) Summary plot of the effect of blocking CaMKIIα on iLTP with bath-applied KN-62 or cell-loaded AIP.

(C) Time course of inhibitory postsynaptic currents evoked by photo-activation of SOM or PV-INs immediately after whole-cell break-in using an internal patch solution that contains calcium and calmodulin. To isolate the effect of CaMKIIα, we blocked the calcium-sensitive phosphatase calcineurin with bath application of cyclosporin A (CyA) throughout the experiment. Average IPSC traces obtained in the first minute (black) and after 20 min (red) of whole-cell patch recording from a single experiment are shown in the insets.

(D) Summary plot of the effect of loading calcium and calmodulin on the amplitude of inhibitory responses elicited by optogenetic activation of SOM- and PV-INs. The IPSC increase observed for SOM-IN inputs is abolished by KN-62. Data are represented as mean ± SEM. Asterisks denote p value of <0.05, Mann-Whitney test.

CaMKIIα is sufficient to potentiate inputs from SOM-INs. In striking contrast, loading the cell with Ca^{2+} and calmodulin had no effect on IPSCs evoked by stimulating PV-INs (Ca^{2+}/calmodulin: 120% ± 9%, n = 8, p = 0.20; Figures 2C and 2D). We confirmed the specificity of these findings by repeating similar experiments but this time loading the PN with a constitutively active CaMKIIα (10 nM CaMKII*) (Tavalin and Colbran, 2017). Again, the amplitude of IPSCs mediated by SOM-INs, but not PV-INs, increased 20 min after whole-cell break-in (SOM: 146% ± 10%, n = 5 cells, p = 0.02; PV: 108% ± 12%, n = 5 cells, p = 0.58; Figure S1). As active CaMKIIα loaded from the pipette fails to potentiate synapses formed by PV-INs, where its concentration is likely highest, but does strengthen inputs from more distal SOM-INs, our results support the hypothesis that the inherent sensitivity to CaMKIIα signaling differs across these distinct GABAergic synaptic populations.

Our results suggest that iLTP induction requires postsynaptic NMDARs, Ca^{2+} influx, and CaMKIIα activation. However, the site of expression remains unclear. Therefore, we first estimated the number and conductance of $GABA_A$ receptors activated by optical stimulation of SOM-INs using non-stationary fluctuation analysis (Clements, 2003) before and after NMDA application (Figure 3A). This approach indicated that NMDAR activation produces an increase in $GABA_A$ receptor number (before: 182 ± 49; after: 370 ± 87, n = 8, p = 0.01), but not conductance (before: 41 ± 9 pS; after: 34 ± 6 pS, n = 8, p = 0.32), suggesting that iLTP involves the addition of $GABA_A$ receptors in the postsynaptic membrane. To test this hypothesis, we pharmacologically blocked SNARE-dependent insertion of receptors by

including botulinum toxin type A (BoNT-A) in the patch pipette and found that this manipulation completely abolished iLTP (Figure 3B). Indeed, IPSCs were slightly reduced following NMDA application in cells loaded with BoNT-A (86% ± 4%, n = 8, p = 0.01) while cells loaded with heat-inactivated BoNT-A (HI-BoNT) still exhibited iLTP (126% ± 3%, n = 7, p = 0.02). These results are consistent with iLTP being mediated by insertion of receptors at either existing or newly formed connections, possibly reflecting the return of recurrent inhibitory synapses (Villa et al., 2016).

Finally, to further test the hypothesis that iLTP is expressed postsynaptically, we bypassed GABA release from presynaptic INs entirely and directly activated postsynaptic $GABA_A$ receptors with photolysis of caged GABA targeting distal PN dendrites (Figure 3C). Consistent with postsynaptic iLTP expression, IPSCs evoked by GABA uncaging also increased following 2 min of NMDA exposure (161% ± 29%, n = 10, p = 0.0009), and this result was blocked by bath application of KN-62 (99% ± 3%, n = 5, p = 0.03 compared to control). In combination, these results strongly indicate that iLTP is both induced and expressed postsynaptically and is restricted to subsets of GABAergic synapses.

We next tested whether glutamatergic synaptic activity can also trigger NMDAR-dependent iLTP by taking advantage of a dual-wavelength optogenetic approach (Figure 4A). Red-shifted tdTomato-tagged ChrimsonR was conditionally expressed in prefrontal SOM-INs, enabling these INs to be activated by 594 nm light (Klapoetke et al., 2014). We also expressed EYFP-tagged ChR2 in the medial dorsal thalamus (MD), the
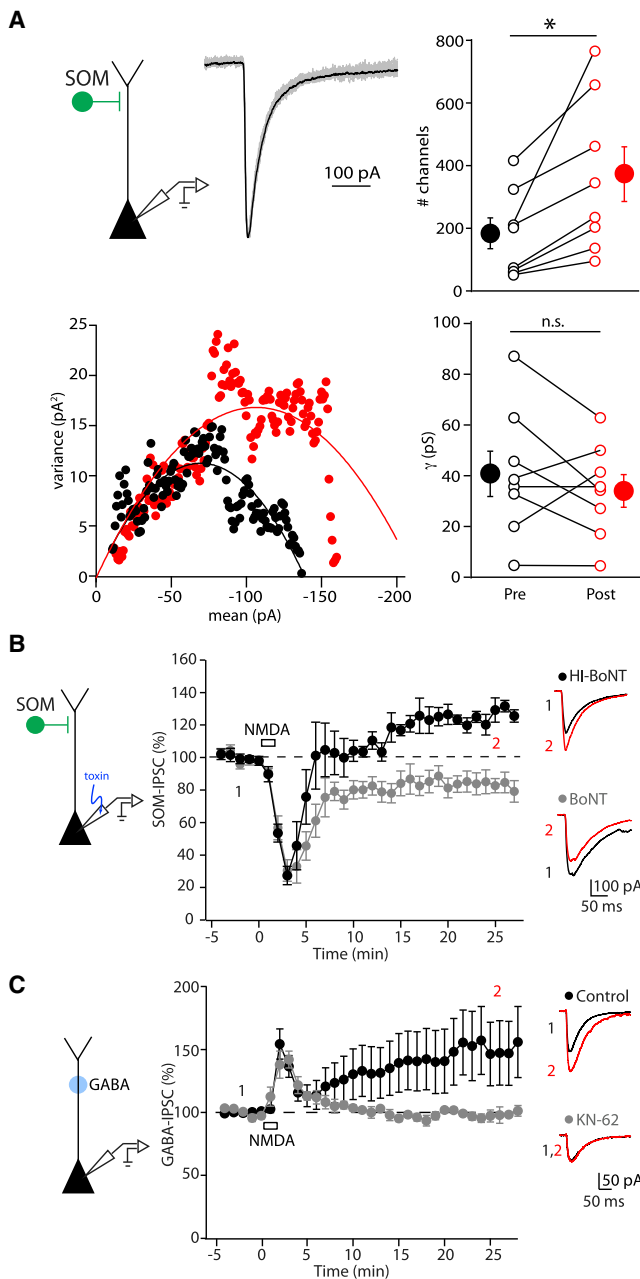
Figure 3. Dendritic iLTP Is Expressed Postsynaptically

(A) Non-stationary fluctuation analysis of inhibitory responses evoked by photo-stimulation of SOM-INs in a representative experiment. Top: example peak-scaled IPSC traces (gray) and average IPSC (black) during the baseline period. Bottom: plot of the variance against the mean IPSC amplitude before (black) and after (red) NMDA application. Right: summary plot of the estimated channel number (top) and conductance (bottom) before and after NMDA application. Asterisks denote p value of <0.05, paired t test.

(B) Time course of inhibitory responses evoked by photo-stimulation of SOM-INs showing that botulinum type A (BoNT-A) abolishes iLTP (gray circles) while the heat-inactivated BoNT-A (black circles) does not. Right: average IPSC traces obtained before (black) and after (red) NMDA exposure from single experiments are shown.

(C) Time course of IPSCs evoked by photolysis of RuBi-GABA at dendritic regions of L2/3 pyramidal cells. Under control conditions, IPSCs elicited by
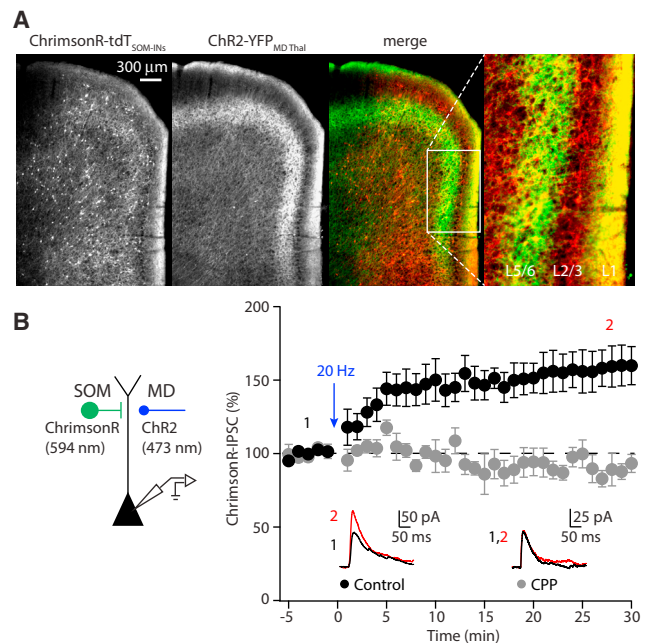

Figure 4. Excitatory Synaptic Stimulation Induces iLTP of SOM-INs

(A) Viral vectors were used to express the red-shifted opsin ChrimsonR-tdTomato in SOM-INs and ChR2-EYFP in MD thalamic afferents, which each target layer 1 in the PFC.

(B) Left: schematic of the experimental paradigm. Right: time course of evoked responses. Blue light (473 nm) 20 Hz stimulation of thalamocortical fibers triggers potentiation of IPSCs evoked by red light (594 nm) stimulation of SOM-INs. Average IPSC traces are shown for representative experiments before (black) and after (red) thalamocortical stimulation in the inset. Note that iLTP is blocked in the presence of the NMDAR antagonist CPP. Data are represented as mean ± SEM.

primary source of thalamocortical afferents to the PFC. In initial experiments, we found that 594 nm stimulation reliably evoked IPSCs when the cell was voltage clamped at +10 mV, while no excitatory postsynaptic currents (EPSCs) were observed at a holding potential of −60 mV, demonstrating a lack of ChR2 activation by the red light. In contrast, 473 nm stimulation reliably evoked EPSCs but also IPSCs that were largely disynaptic in origin (Figure S2).

Recent work demonstrated coherent ~20 Hz activity between MD and the PFC during a working memory task (Bolkan et al., 2017). Based on this model, we found that a brief 2 min train of thalamic stimulation at 20 Hz triggered iLTP of SOM-IPSCs comparable to that seen with bath application of NMDA (158% ± 13%, n = 7, p = 0.002; Figure 4B). We confirmed that iLTP triggered by thalamocortical input also requires NMDARs, as it was abolished by bath application of the NMDAR antagonist CPP (90% ± 7%, n = 6, p = 0.005 compared to control; Figure 4B). Thus, synaptic activation of NMDARs is sufficient to induce potentiation of SOM-IN-mediated IPSCs.

direct stimulation of postsynaptic receptors potentiate following NMDA application (black circles), and iLTP is blocked by KN-62 (gray circles). Right: average IPSC traces obtained before (black) and after (red) NMDA exposure from single experiments are shown. Data are represented as mean ± SEM.
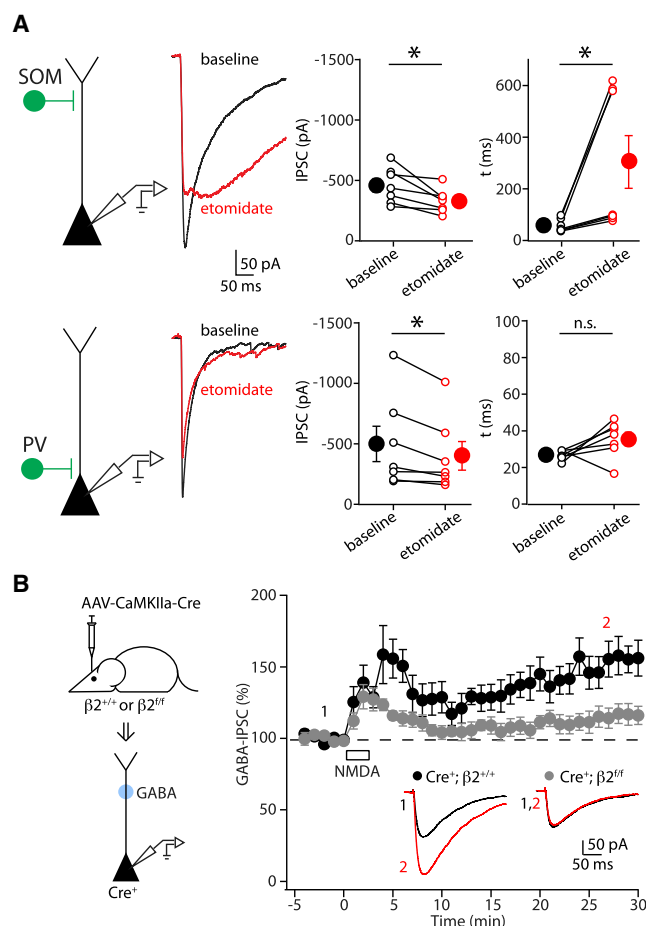
Figure 5. GABA_A Receptor β2 Subunits Are Enriched at Synapses Formed by SOM-INs and Are Required for iLTP

(A) Top: average IPSC traces obtained from optogenetic stimulation of SOM-INs (left) at baseline (black) and in etomidate (red) for a representative experiment. Summary plots of the effect of etomidate on average IPSC amplitude and decay kinetics are shown. Bottom: similar experiments are shown for optogenetic stimulation of PV-INs. Asterisks denote p value of <0.05, paired t test.

(B) Left: schematic of the experimental paradigm. Pyramidal cells expressing EGFP-Cre are targeted for patching, and inhibitory responses are elicited by uncaging GABA in the dendritic regions. Right: time course of the effect of NMDA application on uncaging responses in cells obtained from wild-type (black) or β2-deleted (gray) cells. Average IPSC traces obtained before (black) and after (red) NMDA exposure from a single experiment are shown in the insets. Data are represented as mean ± SEM.

Our results suggest that the molecular constituency of synapses formed by SOM-INs may differ from those formed by other INs, resulting in differential sensitivity to plasticity induction. Indeed, previous studies have linked both β2 and β3 subunits of the GABA_A receptor to iLTP induction in the cerebellum and hippocampal cultures, respectively (He et al., 2015; Petrini et al., 2014). Therefore, we first asked whether functional expression of these subunits might distinguish synapses formed by SOM- versus PV-INs (Figure 5A). Bath application of etomidate, a β2/β3-selective positive allosteric modulator, slightly reduced the amplitude of IPSCs arising from both SOM- and PV-INs

(SOM: −26% ± 6%, n = 7, p = 0.02; PV: −17% ± 4%, n = 7, p = 0.02). However, etomidate substantially slowed the decay of IPSCs evoked by optical stimulation of SOM-INs (baseline: 59 ± 9 ms; etomidate: 308 ± 102 ms, n = 7, p = 0.02) but had no impact on the decay of PV-IN-evoked currents (baseline: 27 ± 1 ms; etomidate: 35 ± 4 ms, n = 7, p = 0.16). The higher sensitivity of synapses formed by SOM-INs versus PV-INs to etomidate suggests that β2/β3 expression is functionally enriched at the former versus the latter.

We then tested whether β2- or β3-containing GABA_A receptors are required for iLTP by using mice expressing floxed conditional alleles of either the β2 (Figures S3A and S3B) or β3 (Ferguson et al., 2007) subunit of the GABA_A receptor. We virally introduced EGFP-tagged Cre recombinase (AAV-CaMKIIα-EGFP-Cre; Figure 5B) into the prefrontal cortex of conditional mice and prepared acute slices 6–7 weeks post-injection (Figure S3C). Notably, genetic deletion of the β2 subunit eliminated iLTP of uncaging-evoked IPSCs following NMDA application (Cre+; β2$^{f/f}$: 115% ± 7%, n = 8, p = 0.08; Figure 5B). In contrast, neither expression of EGFP-Cre by itself (Cre+; β2$^{+/+}$: 161% ± 13%, n = 6, p = 0.03; Figure 5B) nor deletion of the β3 subunit blocked potentiation of uncaging-evoked IPSCs (Cre+; β3$^{f/f}$: 161% ± 21%, n = 7, p = 0.02; Figure S3D).

The preceding results indicate that activation of NMDARs can acutely potentiate the strength of inhibition mediated by selective subsets of GABAergic INs. We next asked whether glutamatergic signaling also plays a role in regulating inhibitory potency *in vivo*. To address this possibility, we utilized a genetic strategy for sparsely eliminating NMDAR signaling in prefrontal neurons in the intact mouse. We used the same viral vector to express EGFP-tagged Cre recombinase in mice harboring a floxed allele of the obligatory GluN1 subunit of the NMDAR (Tsien et al., 1996). In slices prepared 6–7 weeks following injection, infected (EGFP-positive) and non-transfected (EGFP-negative) cells were intermixed. Whole-cell recordings of PN pairs combined with local electrical stimulation confirmed that NMDARs were not functional in Cre-expressing cells (Figures 6A and 6B). In contrast, the amplitude of AMPAR-mediated excitation was not significantly altered by GluN1 deletion (Cre−; GluN1$^{f/f}$: −78.9 ± 9.9 pA, Cre+; GluN1$^{f/f}$: −118.2 ± 29.6 pA, n = 10, p = 0.43; Figures 6A and 6B).

We then examined inhibition onto GluN1-deleted cells. As Cre recombinase was utilized to remove GluN1 expression, we could not adopt the same strategy of ChR2-mediated activation of IN subtypes. To compare inhibition putatively mediated by SOM-INs or PV-INs, we placed a stimulating electrode in either layer 1 or the cell body layer, respectively (Figures 6C and 6D). We further enhanced the selectivity of activation by including either the P/Q-type Ca^{2+} channel blocker agatoxin TK or the N-type channel blocker conotoxin GVIA in the bathing solution to block GABA release from specific INs (Kruglikov and Rudy, 2008). While PV-INs exclusively depend on P/Q-type Ca^{2+} channels for GABA release, SOM-INs utilize both channel types to mediate GABAergic transmission (Figures S4A and S4B). Consistent with our preceding results, GluN1 deletion led to a significant reduction in GABAergic inhibition putatively mediated by SOM-INs (Cre−; GluN1$^{f/f}$: −338.7 ± 100.4 pA, Cre+; GluN1$^{f/f}$: −120 ± 45.1 pA, n = 9, p = 0.004; Figure 6C). Surprisingly, we
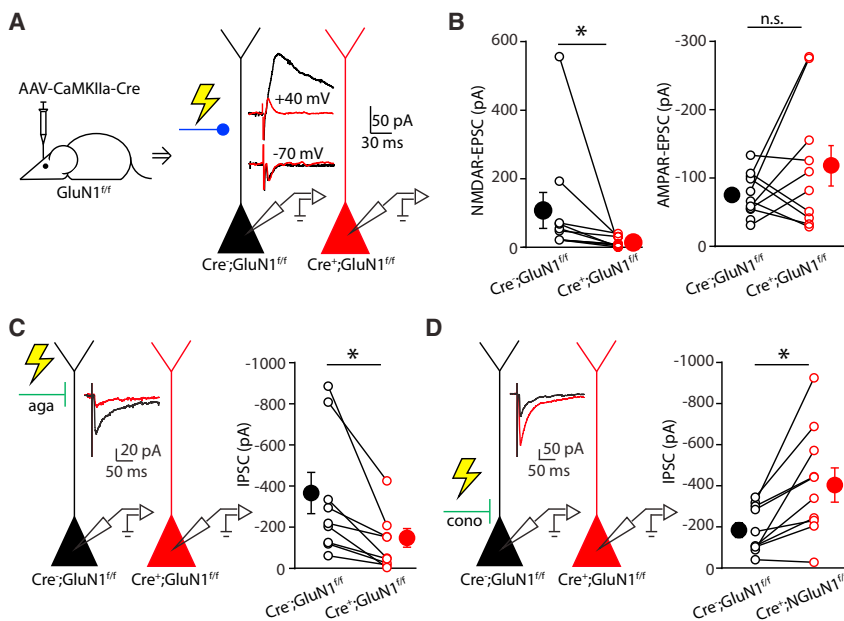
Figure 6. Conditional Deletion of NMDARs Differentially Alters Dendritic and Perisomatic Inhibition

(A) Schematic of whole-cell recordings in neighboring cells to compare evoked glutamatergic responses. AMPAR-EPSCs (−70 mV) and NMDAR-ESPCs (+40 mV) in control (black) and GluN1-lacking (red) cells are shown in the insets.

(B) Summary plot of NMDAR-EPSC (left) and AMPAR-EPSC amplitude (right).

(C) Left: schematic of dual recordings in neighboring cells to compare inhibitory responses evoked by an extracellular stimulating electrode in layer 1. Aga-toxin (aga) was bath applied to block P/Q-type Ca^{2+} channels. Average IPSC traces are shown for a control (black) and a GluN1-lacking (red) cell in a representative experiment. Right: summary plot comparing amplitude of isolated IPSCs between wild-type and GluN1-deleted cells.

(D) Similar results obtained for IPSCs evoked by stimulating in layer 2/3 and in the presence of con-otoxin (cono) to block N-type Ca^{2+} channels. Data are represented as mean ± SEM. Asterisks denote p value of <0.05, Wilcoxon matched-pairs signed rank test.

found that loss of NMDAR signaling produced a significant enhancement of putative PV-IN-mediated inhibition (Cre⁻; GluN1^{f/f}: −187.1 ± 35.8 pA, Cre⁺; GluN1^{f/f}: −411.7 ± 83.2 pA, n = 9, p = 0.004; Figure 6D). These results indicate that NMDARs control the strength of GABAergic inhibition *in vivo*, but the directionality of this influence differs across inhibitory synaptic subpopulations, potentially leading to a disruption of the balance between excitation and inhibition at the subcellular level.

DISCUSSION

The cellular mechanisms underlying the preservation of balance between synaptic excitation and inhibition across distinct GABAergic circuits remain poorly understood. Recent work has begun to focus on GABAergic synaptic plasticity as a key mediator of homeostatic control (Castillo et al., 2011; Kullmann et al., 2012). In this study, we found that activation of glutamatergic NMDARs by either exogenous agonists or endogenous glutamate is capable of potentiating GABAergic synapses in the neocortex. Notably, this form of plasticity is specific to inputs arising from SOM-INs and does not occur for inputs from either PV- or VIP-INs. Using dual-wavelength optogenetic stimulation, we also show that physiologically patterned optogenetic stimulation of excitatory thalamocortical fibers in the PFC is sufficient to induce iLTP. Finally, we find that signaling through NMDARs is necessary for the maintenance of putative SOM-IN synapses. Our results highlight a novel mechanism for maintaining the balance of excitation and inhibition within neocortical dendrites.

Regulation of GABAergic signaling in the neocortex has largely focused on perisomatic inhibition. Work *in vivo* showed that loss of visual stimulation resulted in a strengthening of PV-IN synapses onto layer 4 PNs (Maffei et al., 2006). Similarly, the ratio

of glutamatergic and GABAergic inputs to layer 2/3 PNs in visual cortex is highly conserved despite large variations in the absolute magnitudes of each component (Xue et al., 2014). This balance was attributed to the regulation of synapses formed by PV-INs, as chronically altering PN spike output resulted in a corresponding change in perisomatic inhibition (Xue et al., 2014). In keeping with this observation, several studies demonstrated modulation of PV-IN inputs following alterations in pyramidal cell firing (Bartley et al., 2008; Holmgren and Zilberter, 2001). Indeed, postsynaptic spiking is sufficient to induce changes in inhibitory synaptic efficacy from fast-spiking, putative PV-expressing INs (Kurotani et al., 2008; Lourenço et al., 2014). Overall, these findings suggest a direct linkage of PN *output* and the strength of *perisomatic* inhibition.

In contrast to these studies, our results indicate a distinct relationship between excitation and inhibition, where glutamatergic *input* is coupled to the strength of *dendritic* GABAergic signaling. Supporting this idea, the coupling of NMDARs with GABAergic plasticity was previously shown in cultured hippocampal neurons (Marsden et al., 2007; Petrini et al., 2014), though input specificity was not addressed. Surprisingly, hippocampal iLTP was shown to require the β3 GABA_A subunit (Petrini et al., 2014), indicating that not all aspects of this phenomenon may be conserved. Nevertheless, it is intriguing to speculate that dendritic iLTP may be a general process across cortical areas. Given the dependence of SOM-IN iLTP on NMDAR-mediated Ca^{2+} influx, we predict that this form of plasticity will be highly localized in small dendritic regions, consistent with the compartmentalization of glutamatergic Ca^{2+} transients (Higley and Sabatini, 2008; Sabatini et al., 2002). We previously showed that inhibition mediated by SOM-INs could, in turn, influence excitatory transmission and Ca^{2+} signaling at the scale of single dendritic spines (Chiu et al., 2013), potentially driving long-term depression of glutamatergic inputs and regulating

spine stability (Chen et al., 2015; Hayama et al., 2013). Thus, the homeostatic interaction of glutamatergic and GABAergic signaling may fine-tune excitatory synaptic integration at the level of individual synapses.

The critical role of inhibitory plasticity *in vivo* is also supported by recent work showing that GABAergic synapses formed in the dendrites of L2/3 PNs of visual cortex are highly dynamic both spontaneously and in response to altered sensory experience (Chen et al., 2012; Kannan et al., 2016; Villa et al., 2016). Notably, GABAergic inputs to distal dendrites exhibit greater turnover than more proximal contacts, with synapses on dendritic spines among the most labile (Chen et al., 2012). This observation is consistent with our earlier findings that SOM-INs make a subset of their inputs directly onto spine heads (Chiu et al., 2013). Given these results and our present findings, it would be interesting to examine the role of NMDARs in visual experience-dependent reorganization of cortical GABAergic circuits.

The selective induction of NMDAR- and CaMKIIα-dependent iLTP at synapses formed by SOM-INs might be solely explained by their structural proximity to glutamatergic inputs that also target PN dendrites. However, two results argue for a more complex explanation. First, loading either activated calmodulin or CaMKIIα through the patch pipette was insufficient to trigger iLTP at PV-IN synapses despite robustly potentiating inputs from SOM-INs. Second, application of the β2/β3 subunit containing GABAergic receptor modulator etomidate selectively altered currents evoked by stimulation of SOM-INs, while genetic deletion of the β2 subunit prevented induction of iLTP. Overall, these results suggest the tantalizing hypothesis that the molecular constituency of GABAergic synapses might differ across the somatodendritic arbor. The mechanisms underlying this molecular heterogeneity are unclear and could involve the differential trafficking of receptor subunits and accessory molecules to distinct pools of synapses across the somatodendritic arbor. In contrast to glutamatergic synapses, the structural organization of GABAergic inputs is not well characterized. Previous work has suggested the possibility that inhibitory scaffolding molecules may vary across synaptic subpopulations. In the neocortex, the cell adhesion molecule neuroligin-2 was reported to be necessary for synapses formed by PV-INs, but not SOM-INs (Gibson et al., 2009). In the cerebellum, the scaffolding molecule gephyrin was suggested to be critical for dendritic, but not perisomatic, GABAergic inputs to Purkinje cells (Viltono et al., 2008). Recent studies have begun to reveal additional molecules involved in the structure and function of inhibitory synapses (Uezu et al., 2016; Yamasaki et al., 2017), and future investigation will be necessary to determine their selective roles in different cellular compartments.

Previous models of synaptic homeostasis often rely on a straightforward "balance" of overall excitation and inhibition that may be oversimplified. As we have shown, dysregulation of NMDAR signaling results in opposite alterations in putative PV- and SOM-IN-mediated inhibition. Importantly, these experiments do not rule out non-synaptic explanations for the links between NMDARs and GABAergic inputs *in vivo*. However, they are consistent with our iLTP data and highlight the possibility that the strength of inhibition can be redistributed along the somatodendritic axis in response to altered glutamatergic signaling. Indeed,

many studies have suggested that the functional roles of inhibition mediated by different IN populations are highly distinct (Atallah et al., 2012; Lee et al., 2012; Wilson et al., 2012). Thus, although the total amount of inhibition may remain "balanced," the functional consequences for cellular and circuit activity may be considerable.

In conclusion, we present evidence for a novel synapse-specific mechanism for linking excitatory signaling to the potency of dendritic GABAergic inhibition. We expect that future studies into the cellular mechanisms governing such specificity will yield rich rewards into understanding both basic synaptic development and maintenance as well as circuit organization and function.

STAR★METHODS

Detailed methods are provided in the online version of this paper and include the following:

- KEY RESOURCES TABLE
- CONTACT FOR REAGENT AND RESOURCE SHARING
- EXPERIMENTAL MODEL AND SUBJECT DETAILS
- METHOD DETAILS
  - Slice Preparation
  - Electrophysiology
  - Synaptic Stimulation and GABA Uncaging
  - Conditional Deletion of Targeted Receptor Subunits
  - Generation of Conditional β2 Knockout Mice
  - Pharmacology
  - Slice Resectioning for Immunofluorescence
- QUANTIFICATION AND STATISTICAL ANALYSIS

REFERENCES

Ascoli, G.A., Alonso-Nanclares, L., Anderson, S.A., Barrionuevo, G., Benavides-Piccione, R., Burkhalter, A., Buzsáki, G., Cauli, B., Defelipe, J., Fairén, A., et al.; Petilla Interneuron Nomenclature Group (2008). Petilla terminology: nomenclature of features of GABAergic interneurons of the cerebral cortex. Nat. Rev. Neurosci. *9*, 557–568.

Atallah, B.V., Bruns, W., Carandini, M., and Scanziani, M. (2012). Parvalbumin-expressing interneurons linearly transform cortical responses to visual stimuli. Neuron *73*, 159–170.

Bartley, A.F., Huang, Z.J., Huber, K.M., and Gibson, J.R. (2008). Differential activity-dependent, homeostatic plasticity of two neocortical inhibitory circuits. J. Neurophysiol. *100*, 1983–1994.

Bolkan, S.S., Stujenske, J.M., Parnaudeau, S., Spellman, T.J., Rauffenbart, C., Abbas, A.I., Harris, A.Z., Gordon, J.A., and Kellendonk, C. (2017). Thalamic projections sustain prefrontal activity during working memory maintenance. Nat. Neurosci. *20*, 987–996.

Cardin, J.A., Carlén, M., Meletis, K., Knoblich, U., Zhang, F., Deisseroth, K., Tsai, L.H., and Moore, C.I. (2009). Driving fast-spiking cells induces gamma rhythm and controls sensory responses. Nature *459*, 663–667.

Castillo, P.E., Chiu, C.Q., and Carroll, R.C. (2011). Long-term plasticity at inhibitory synapses. Curr. Opin. Neurobiol. *21*, 328–338.

Chen, J.L., Villa, K.L., Cha, J.W., So, P.T., Kubota, Y., and Nedivi, E. (2012). Clustered dynamics of inhibitory synapses and dendritic spines in the adult neocortex. Neuron *74*, 361–373.

Chen, S.X., Kim, A.N., Peters, A.J., and Komiyama, T. (2015). Subtype-specific plasticity of inhibitory circuits in motor cortex during motor learning. Nat. Neurosci. *18*, 1109–1115.

Chiu, C.Q., Lur, G., Morse, T.M., Carnevale, N.T., Ellis-Davies, G.C., and Higley, M.J. (2013). Compartmentalization of GABAergic inhibition by dendritic spines. Science *340*, 759–762.

Clements, J.D. (2003). Variance-mean analysis: a simple and reliable approach for investigating synaptic transmission and modulation. J. Neurosci. Methods *130*, 115–125.

Ferguson, C., Hardy, S.L., Werner, D.F., Hileman, S.M., Delorey, T.M., and Homanics, G.E. (2007). New insight into the role of the beta3 subunit of the GABAA-R in development, behavior, body weight regulation, and anesthesia revealed by conditional gene knockout. BMC Neurosci. *8*, 85.

Fu, Y., Tucciarone, J.M., Espinosa, J.S., Sheng, N., Darcy, D.P., Nicoll, R.A., Huang, Z.J., and Stryker, M.P. (2014). A cortical circuit for gain control by behavioral state. Cell *156*, 1139–1152.

Gibson, J.R., Huber, K.M., and Südhof, T.C. (2009). Neuroligin-2 deletion selectively decreases inhibitory synaptic transmission originating from fast-spiking but not from somatostatin-positive interneurons. J. Neurosci. *29*, 13883–13897.

Gogolla, N., Leblanc, J.J., Quast, K.B., Südhof, T.C., Fagiolini, M., and Hensch, T.K. (2009). Common circuit defect of excitatory-inhibitory balance in mouse models of autism. J. Neurodev. Disord. *1*, 172–181.

Hayama, T., Noguchi, J., Watanabe, S., Takahashi, N., Hayashi-Takagi, A., Ellis-Davies, G.C., Matsuzaki, M., and Kasai, H. (2013). GABA promotes the competitive selection of dendritic spines by controlling local Ca2+ signaling. Nat. Neurosci. *16*, 1409–1416.

He, Q., Duguid, I., Clark, B., Panzanelli, P., Patel, B., Thomas, P., Fritschy, J.M., and Smart, T.G. (2015). Interneuron- and GABA(A) receptor-specific inhibitory synaptic plasticity in cerebellar Purkinje cells. Nat. Commun. *6*, 7364.

Higley, M.J., and Sabatini, B.L. (2008). Calcium signaling in dendrites and spines: practical and functional considerations. Neuron *59*, 902–913.

Holmgren, C.D., and Zilberter, Y. (2001). Coincident spiking activity induces long-term changes in inhibition of neocortical pyramidal cells. J. Neurosci. *21*, 8270–8277.

Isaacson, J.S., and Scanziani, M. (2011). How inhibition shapes cortical activity. Neuron *72*, 231–243.

Kannan, M., Gross, G.G., Arnold, D.B., and Higley, M.J. (2016). Visual deprivation during the critical period enhances layer 2/3 GABAergic inhibition in mouse V1. J. Neurosci. *36*, 5914–5919.

Klapoetke, N.C., Murata, Y., Kim, S.S., Pulver, S.R., Birdsey-Benson, A., Cho, Y.K., Morimoto, T.K., Chuong, A.S., Carpenter, E.J., Tian, Z., et al. (2014). Independent optical excitation of distinct neural populations. Nat. Methods *11*, 338–346.

Kruglikov, I., and Rudy, B. (2008). Perisomatic GABA release and thalamocortical integration onto neocortical excitatory cells are regulated by neuromodulators. Neuron *58*, 911–924.

Kullmann, D.M., Moreau, A.W., Bakiri, Y., and Nicholson, E. (2012). Plasticity of inhibition. Neuron *75*, 951–962.

Kurotani, T., Yamada, K., Yoshimura, Y., Crair, M.C., and Komatsu, Y. (2008). State-dependent bidirectional modification of somatic inhibition in neocortical pyramidal cells. Neuron *57*, 905–916.

Lee, S.H., Földy, C., and Soltesz, I. (2010). Distinct endocannabinoid control of GABA release at perisomatic and dendritic synapses in the hippocampus. J. Neurosci. *30*, 7993–8000.

Lee, S.H., Kwan, A.C., Zhang, S., Phoumthipphavong, V., Flannery, J.G., Masmanidis, S.C., Taniguchi, H., Huang, Z.J., Zhang, F., Boyden, E.S., et al. (2012). Activation of specific interneurons improves V1 feature selectivity and visual perception. Nature *488*, 379–383.

Lewis, D.A., and Hashimoto, T. (2007). Deciphering the disease process of schizophrenia: the contribution of cortical GABA neurons. Int. Rev. Neurobiol. *78*, 109–131.

Lourenço, J., Pacioni, S., Rebola, N., van Woerden, G.M., Marinelli, S., DiGregorio, D., and Bacci, A. (2014). Non-associative potentiation of perisomatic inhibition alters the temporal coding of neocortical layer 5 pyramidal neurons. PLoS Biol. *12*, e1001903.

Maffei, A., Nataraj, K., Nelson, S.B., and Turrigiano, G.G. (2006). Potentiation of cortical inhibition by visual deprivation. Nature *443*, 81–84.

Malenka, R.C., and Bear, M.F. (2004). LTP and LTD: an embarrassment of riches. Neuron *44*, 5–21.

Marsden, K.C., Beattie, J.B., Friedenthal, J., and Carroll, R.C. (2007). NMDA receptor activation potentiates inhibitory transmission through GABA receptor-associated protein-dependent exocytosis of GABA(A) receptors. J. Neurosci. *27*, 14326–14337.

Mishina, M., and Sakimura, K. (2007). Conditional gene targeting on the pure C57BL/6 genetic background. Neurosci. Res. *58*, 105–112.

Murayama, M., Pérez-Garci, E., Nevian, T., Bock, T., Senn, W., and Larkum, M.E. (2009). Dendritic encoding of sensory stimuli controlled by deep cortical interneurons. Nature *457*, 1137–1141.

Petrini, E.M., Ravasenga, T., Hausrat, T.J., Iurilli, G., Olcese, U., Racine, V., Sibarita, J.B., Jacob, T.C., Moss, S.J., Benfenati, F., et al. (2014). Synaptic recruitment of gephyrin regulates surface GABAA receptor dynamics for the expression of inhibitory LTP. Nat. Commun. *5*, 3921.

Pfeffer, C.K., Xue, M., He, M., Huang, Z.J., and Scanziani, M. (2013). Inhibition of inhibition in visual cortex: the logic of connections between molecularly distinct interneurons. Nat. Neurosci. *16*, 1068–1076.

Pologruto, T.A., Sabatini, B.L., and Svoboda, K. (2003). ScanImage: flexible software for operating laser scanning microscopes. Biomed. Eng. Online *2*, 13.

Pouille, F., and Scanziani, M. (2001). Enforcement of temporal fidelity in pyramidal cells by somatic feed-forward inhibition. Science *293*, 1159–1163.

Rial Verde, E.M., Zayat, L., Etchenique, R., and Yuste, R. (2008). Photorelease of GABA with visible light using an inorganic caging group. Front. Neural Circuits *2*, 2.

Rudy, B., Fishell, G., Lee, S., and Hjerling-Leffler, J. (2011). Three groups of interneurons account for nearly 100% of neocortical GABAergic neurons. Dev. Neurobiol. *71*, 45–61.

Sabatini, B.L., Oertner, T.G., and Svoboda, K. (2002). The life cycle of Ca(2+) ions in dendritic spines. Neuron *33*, 439–452.

Taniguchi, H., He, M., Wu, P., Kim, S., Paik, R., Sugino, K., Kvitsiani, D., Fu, Y., Lu, J., Lin, Y., et al. (2011). A resource of Cre driver lines for genetic targeting of GABAergic neurons in cerebral cortex. Neuron *71*, 995–1013.

Tavalin, S.J., and Colbran, R.J. (2017). CaMKII-mediated phosphorylation of GluN2B regulates recombinant NMDA receptor currents in a chloride-dependent manner. Mol. Cell. Neurosci. *79*, 45–52.

Tsien, J.Z., Chen, D.F., Gerber, D., Tom, C., Mercer, E.H., Anderson, D.J., Mayford, M., Kandel, E.R., and Tonegawa, S. (1996). Subregion- and cell type-restricted gene knockout in mouse brain. Cell *87*, 1317–1326.

Turrigiano, G. (2011). Too many cooks? Intrinsic and synaptic homeostatic mechanisms in cortical circuit refinement. Annu. Rev. Neurosci. *34*, 89–103.

Uezu, A., Kanak, D.J., Bradshaw, T.W., Soderblom, E.J., Catavero, C.M., Burette, A.C., Weinberg, R.J., and Soderling, S.H. (2016). Identification of an elaborate complex mediating postsynaptic inhibition. Science *353*, 1123–1129.

van Versendaal, D., Rajendran, R., Saiepour, M.H., Klooster, J., Smit-Rigter, L., Sommeijer, J.P., De Zeeuw, C.I., Hofer, S.B., Heimel, J.A., and Levelt, C.N. (2012). Elimination of inhibitory synapses is a major component of adult ocular dominance plasticity. Neuron *74*, 374–383.

Villa, K.L., Berry, K.P., Subramanian, J., Cha, J.W., Chan Oh, W., Kwon, H.B., Kubota, Y., So, P.T., and Nedivi, E. (2016). Inhibitory synapses are repeatedly assembled and removed at persistent sites in vivo. Neuron *90*, 662–664.

Viltono, L., Patrizi, A., Fritschy, J.M., and Sassoè-Pognetto, M. (2008). Synaptogenesis in the cerebellar cortex: differential regulation of gephyrin and GABAA receptors at somatic and dendritic synapses of Purkinje cells. J. Comp. Neurol. *508*, 579–591.

Wang, J.H., and Kelly, P.T. (1995). Postsynaptic injection of CA2+/CaM induces synaptic potentiation requiring CaMKII and PKC activity. Neuron *15*, 443–452.

Wilson, N.R., Runyan, C.A., Wang, F.L., and Sur, M. (2012). Division and subtraction by distinct cortical inhibitory networks in vivo. Nature *488*, 343–348.

Xue, M., Atallah, B.V., and Scanziani, M. (2014). Equalizing excitation-inhibition ratios across visual cortical neurons. Nature *511*, 596–600.

Yamasaki, T., Hoyos-Ramirez, E., Martenson, J.S., Morimoto-Tomita, M., and Tomita, S. (2017). GARLH family proteins stabilize GABAA receptors at synapses. Neuron *93*, 1138–1152.e6.

STAR★METHODS

KEY RESOURCES TABLE

REAGENT or RESOURCE	SOURCE	IDENTIFIER
Antibodies		
Rabbit anti-RFP polyclonal	Rockland Immunochemicals	600-401-379; RRID: AB_2209751
Chicken anti-GFP polyclonal	Rockland Immunochemicals	600-901-215S; RRID: AB_1537403
Rabbit anti-GFP polyclonal	Invitrogen	A-6455; RRID: AB_221570
Goat anti-rabbit Alexa 555 secondary	Invitrogen	A-21428; RRID: AB_141784
Goat anti-chicken Alexa 488 secondary	Invitrogen	A-11039; RRID: AB_142924
Goat anti-rabbit Alexa 488 secondary	Invitrogen	A-11008; RRID: AB_143165
Bacterial and Virus Strains		
AAV5-EF1a-DIO-hChR2(H134R)-EYFP	UNC Vector Core	N/A
AAV8-CAG-FLEX-ChrimsonR-tdTomato	Addgene	N/A
AAV-hSyn-hChR2(H134R)-EYFP	UNC Vector Core	N/A
AAV8-CaMKII-EGFP-Cre	UNC Vector Core	N/A
Chemicals, Peptides, and Recombinant Proteins		
KN-62	Tocris	1277
ω-Agatoxin TK	Peptides International	4294 s
ω-Conotoxin GVIA	Peptides International	4161-v
Calmodulin, Bovine Brain	Calbiochem	208690-1MG
constitutively active CaMKII*	S.J. Tavalin; Tavalin and Colbran, 2017	N/A
Experimental Models: Organisms/Strains		
Mouse: SOM-Cre (Sst$^{tm2.1(cre)Zjh}$/J)	The Jackson Laboratory	RRID: IMSR_JAX:013044
Mouse: PV-Cre (Pvalb$^{tm1(cre)Arbr}$/J)	The Jackson Laboratory	RRID: IMSR_JAX:008069
Mouse: VIP-Cre (Vip$^{tm1(cre)Zjh}$/J)	The Jackson Laboratory	RRID: IMSR_JAX:010908
Mouse: GluN1$^{fl/fl}$ (B6.129S4-Grin1^{tm2Stl}/J)	The Jackson Laboratory	RRID: IMSR_JAX:005246
Mouse: Gabrb3$^{fl/fl}$ (B6;129-Gabrb3$^{tm2.1Geh}$/J)	The Jackson Laboratory	RRID: IMSR_JAX:008310
Mouse: Gabrb2$^{fl/fl}$	This paper	N/A

CONTACT FOR REAGENT AND RESOURCE SHARING

Further information and requests for resources and reagents should be directed to and will be fulfilled by the Lead Contact, Michael J. Higley (m.higley@yale.edu).

EXPERIMENTAL MODEL AND SUBJECT DETAILS

All animal handling was performed according to the regulations of the Yale Institutional Animal Care and Use Committee. For all experiments, we used both male and female mice. Mice were housed in a Yale University School of Medicine animal facility on an alternating 12-hour light-dark cycle and provided with food and water *ad libitum*. Optogenetic experiments were performed in acute prefrontal cortical (PFC) slices taken from specific interneuron Cre-driver lines (SOM-Cre, PV-Cre or VIP-Cre mice) (Taniguchi et al., 2011) at postnatal day (P) 30-50 expressing ChR2 or ChrimsonR in targeted IN populations. Control experiments were performed in an interleaved fashion in slices from the same animal on the same day. GABA uncaging experiments were conducted using cortical slices from wild-type C57/Bl6 mice (P30-50) or transgenic mice harboring floxed alleles of Gabrb2 or Gabrb3 (P55-70). Littermate controls were used without regard to sex. Extracellular stimulating electrodes were used to assess basal synaptic transmission in slices from transgenic mice harboring floxed alleles of GluN1 (P55-70). Recordings from control cells were obtained in the same experiment using the same cortical slice.

METHOD DETAILS

Slice Preparation

Under isoflurane anesthesia, mice were decapitated and coronal slices (300 μm thick) were cut in ice-cold external solution containing (in mM): 100 choline chloride, 25 NaHCO$_3$, 1.25 NaH$_2$PO$_4$, 2.5 KCl, 7 MgCl$_2$, 0.5 CaCl$_2$, 15 glucose, 11.6 sodium ascorbate and 3.1 sodium pyruvate, bubbled with 95% O$_2$ and 5% CO$_2$. Slices containing the prelimbic-infralimbic regions of the PFC were then transferred to artificial cerebrospinal fluid (ACSF) containing (in mM): 127 NaCl, 25 NaHCO3, 1.25 NaH2PO4, 2.5 KCl, 1 MgCl2, 2 CaCl2 and 15 glucose, bubbled with 95% O2 and 5% CO2. After an incubation period of 30 min at 34°C, the slices were maintained at 22–24°C for at least 20 min before use.

Electrophysiology

Experiments were conducted at room temperature (22–24°C) in a submersion-type recording chamber. Whole-cell voltage-clamp recordings were obtained from layer 2/3 pyramidal cells located 200-300 μm from the pial surface and identified with video infrared differential interference contrast. To obtain measurable GABA$_A$R responses at a membrane holding potential of -70 mV, glass electrodes (3.0-3.2 MΩ) were filled with a high chloride internal solution containing (in mM): 100 CsCl, 30 CsGluconate, 10 HEPES, 4 MgCl$_2$, 4 Na$_2$ATP, 0.4 NaGTP and 10 sodium creatine phosphate, adjusted to pH 7.3 with CsOH. In GABA uncaging experiments, red-fluorescent Alexa Fluor-594 (10 μM)(Invitrogen) was included in the pipette solution to visualize cell morphology. For all recordings, series resistance was 15-25 MΩ and uncompensated. Recordings were discarded if series resistance changed >15% during the experiment. Electrophysiological recordings were made using a Multiclamp 700B amplifier (Molecular Devices), filtered at 4 kHz, and digitized at 10 kHz using acquisition software written in MATLAB (Mathworks) (Pologruto et al., 2003).

Synaptic Stimulation and GABA Uncaging

To photoactivate specific INs, SOM-Cre, PV-Cre or VIP-Cre mice were injected at P14-25 into the PFC with recombinant AAV driving Cre-dependent expression of either a ChR2-EYFP or ChrimsonR-tdTomato fusion protein (AAV5-Ef1α-DIO-ChR2-EYFP, University of North Carolina Vector Core or AAV5-CAG-DIO-ChrimsonR-tdTomato, Addgene). To photoactivate thalamic fibers, mice were injected into MD with AAV driving non-conditional expression of ChR2-EYFP. Mice were sacrificed 14-25 days post-injection for slice preparation as described above. To activate opsin-positive cells or fibers, we filled the back aperture of the microscope objective (60x, 1.0 NA, Olympus) with blue (473 nm) or red (594 nm) light from fiber-coupled 473 nm or 594 nm lasers (Spectra Physics), yielding a $\sim$15-20 μm diameter disc of light at the focal plane. A brief (0.5-3 ms) pulse of light (3-5 mW at the sample) reliably stimulated ChR2- and ChrimsonR-expressing cells/fibers and evoked EPSCs or IPSCs in pyramidal neurons. To photorelease GABA, 11 μM Rubi-GABA (Chiu et al., 2013; Rial Verde et al., 2008) was included in the bathing ACSF and the microscope objective was centered over the apical dendritic arbor of the recorded neuron. Light pulses were delivered as with optogenetic stimulation and reliably evoked IPSCs. For experiments involving local electrical stimulation, a glass theta stimulating electrode was placed in layer 1 or 2/3 to evoke IPSCs in distal or perisomatic regions, respectively.

Conditional Deletion of Targeted Receptor Subunits

To remove functional NMDARs, mice harboring a floxed allele of GluN1 (Tsien et al., 1996) (P14-20) were injected into the PFC with AAV driving expression of a Cre-EGFP fusion protein under the CaMKIIα promoter (AAV-CaMKIIα-Cre-EGFP) (University of North Carolina Vector Core). Virus was diluted 1:10 and injected at a volume of 1 μL to obtain sparse infection. Mice were sacrificed 6-7 weeks post-injection for slice preparation as described above. A similar approach was used to delete the GABA$_A$ receptor β2 (see below) or β3 (Ferguson et al., 2007) subunit.

Generation of Conditional β2 Knockout Mice

A BAC clone containing the GABA$_A$R β2 gene (Gabrb2) from C57BL/6 mice genomic DNA was purchased from BACPAC Resources Center (Oakland, CA USA). We combined MultiSite Gateway cloning technology (Invitrogen, Carlsbad, CA USA) and Red/ET-mediated homologous recombination (Gene Bridges GmbH, Heidelberg, Germany) for targeting vector construction. The targeting vector was linearized, electroporated into the embryonic stem (ES) cell line RENKA derived from the C57BL/6N strain (Mishina and Sakimura, 2007), and selected by G418. Recombinant clones were identified by Southern blot analysis using the *Gabrb2* 5′ probe on Spe I-digested genomic DNA, and the *Gabrb2* 3′ probe on BamH I-digested genomic DNA. Targeted clones were injected into eight-cell stage embryos of a CD-1 mouse strain. The embryos were cultured to blastocysts and transferred to pseudopregnant CD-1 mice. Resulting male chimeric mice were crossed with female C57BL/6N mice. After Cre-loxP recombination, the elimination of exon 4 results in a frameshift mutation in the gene encoding GABA$_A$R β2.

Pharmacology

For most experiments (excluding thalamic stimulation experiments), the ACSF included 10 μM NBQX to block AMPA receptors. In a subset of experiments (see text), the ACSF also included (in μM): 6 ifenprodil, 3 CGP-55845, 3 nimodipine, 5 KN-62, 20 cyclosporine A, 100 (S)-MCPG, 50 CPP, 0.5 etomidate, 0.2 ω-agatoxin TK or 1 ω-conotoxin GVIA. In cell loading experiments, the drug concentrations (in μM unless indicated otherwise) are as follows: 500 MK-801, 10 mM BAPTA, 10 AIP, 40/10 Ca^{2+}/calmodulin or 200 ng/ml BoNT-A.

For loading constitutively active CaMKII*, the compound was synthesized as previously described (Tavalin and Colbran, 2017) and added to the internal solution (10 nM). All compounds other than CaMKII* were purchased from Tocris except for conotoxin (Peptides International), agatoxin (Peptides International), and calmodulin (Sigma-Aldrich).

Slice Resectioning for Immunofluorescence

Brain slices were fixed after recording in 4% formaldehyde in phosphate buffer (PBS) for 1 hr at 4°C and then stored in PBS overnight. Post-fixed slices were embedded in 10% gelatin at 4°C and re-sectioned to 50 μm on a vibratome. Slices were incubated in blocking solution containing 10% normal goat serum, 1% bovine serum albumin, and 0.1% Triton X-100 for 1.5 hr at 4°C prior to immunostaining. To visualize ChR2-EYFP in SOM-INs, a primary antibody made in rabbit against green fluorescent protein (GFP) (Invitrogen A6455, 1:500) was applied overnight at 4°C. Sections were then stained with Alexa 488-conjugated secondary antibody (Invitrogen A11008, 1:300) for 4 hr at RT°, rinsed repeatedly with buffer, and mounted on microscope slides for epifluorescence imaging. To visualize both ChrimsonR-tdT in SOM-INs and ChR2-EYFP in thalamic afferents, we used chicken anti-GFP (Rockland 600-901-215S, 1:300) and rabbit anti-RFP (Rockland 600-401-379, 1:300). Sections were stained with Alexa 488-conjugated secondary antibody (Invitrogen A11039, 1:300) and Alexa 555-conjugated secondary antibody (Invitrogen A21428, 1:300). Immunofluorescence images were acquired using an Olympus epifluorescence microscope with a 10x objective.

QUANTIFICATION AND STATISTICAL ANALYSIS

Offline analysis of electrophysiological recordings was performed using custom routines written in IgorPro (Wavemetrics). IPSC amplitudes were calculated by finding the peak of the current traces and averaging the values within a 1 ms window. Potentiation of GABAergic responses was assessed by comparing the average IPSC amplitude in the first 5 min prior to NMDA application or thalamic stimulation to the average IPSC amplitude 20–25 min after plasticity induction for each experiment, using paired Student's t tests at a significance level of $p < 0.05$ in GraphPad Prism 7. To assess the effect of pharmacological blockade on iLTP, we performed Mann-Whitney tests comparing drug versus control experiments. For recordings comparing pairs of neighboring GluN1-positive and -negative cells, a Wilcoxon matched-pairs signed rank test was performed to assess significance at $p < 0.05$ due to non-normally distributed data. Data are represented as mean ± SEM throughout the main text and in all figures. N represents the number of cells, and on average 2-3 cells were obtained from a single animal.